KAPL-P-000082
(K98072)

CONF-9805146--

RECENT PROGRESS IN GaInAsSb THERMOPHOTOVOLTAICS GROWN BY ORGANOMETALLIC VAPOR PHASE EPITAXY

C. A. Wang, H.K. Choi, D. C. Oakley, G. W. Charache

June 1998

NOTICE

KAPL ATOMIC POWER LABORATORY SCHENECTADY, NEW YORK 12301

Operated for the U. S. Department of Energy
by KAPL, Inc. a Lockheed Martin company

DISCLAIMER

Recent Progress in GaInAsSb Thermophotovoltaics Grown by Organometallic Vapor Phase Epitaxy*

C.A. Wang†, H.K. Choi, D.C. Oakley
Lincoln Laboratory, Massachusetts Institute of Technology, Lexington, MA 02173-9108
G.W. Charache
Lockheed Martin, Inc., Schenectaday, NY 12301

Abstract

Studies on the materials development of $Ga_{1-x}In_xAs_ySb_{1-y}$ alloys for thermophotovoltaic (TPV) devices are reviewed. $Ga_{1-x}In_xAs_ySb_{1-y}$ epilayers were grown lattice matched to GaSb substrates by organometallic vapor phase epitaxy (OMVPE) using all organometallic precursors including triethylgallium, trimethylindium, tertiarybutylarsine, and trimethylantimony with diethyltellurium and dimethylzinc as the n- and p-type dopants, respectively. The overall material quality of these alloys depends on growth temperature, In content, V/III ratio, substrate misorientation, and to a lesser extent, growth rate. A mirror-like surface morphology and room temperature photoluminescence (PL) are obtained for GaInAsSb layers with peak emission in the wavelength range between 2 and 2.5 μm. The crystal quality improves for growth temperature decreasing from 575 to 525°C, and with decreasing In content, as based on epilayer surface morphology and low temperature PL spectra. A trend of smaller full width at half-maximum for low temperature PL spectra is observed as the growth rate is increased from 1.5 to 2.5 and 5 μm/h. In general, GaInAsSb layers grown on (100) GaSb substrates with a 6° toward (111)B misorientation exhibited overall better material quality than layers grown on the more standard substrate (100) 2° toward (110). Consistent growth of high performance lattice-matched GaInAsSb TPV devices is also demonstrated.

*This work was sponsored by the Department of Energy under AF Contract No. F19628-95-C-0002. The opinions, interpretations, conclusions and recommendations are those of the author and are not necessarily endorsed by the United States Air Force.
†Fax: 781-981-0122; e-mail: wang@ll.mit.edu.

1. Introduction

Thermophotovoltaic (TPV) power generation involves the conversion of thermal energy to electrical energy through the use of photovoltaic (PV) cells. A critical factor in determining overall system efficiency is optimum utilization of radiant photons: the peak in emissive power of the thermal source should closely match the energy gap of the PV cell material, and photons with energies below semiconductor bandgap should be reflected back to the thermal emitter. The early developments of TPV systems in the 1970's mainly utilized conventional Si solar cells, which were readily available. Consequently, high emitter temperatures in excess of 2000 K are necessary for these cells. Unfortunately, it is difficult to obtain such temperatures with conventional combustion sources, and thermal management of these high temperatures is challenging. As a result, the technology was limited and interest in TPV's declined in the 1980's.

Presently, however, there is strong renewed interest in TPV's because of recent improvements in the quality of epitaxially grown, low energy gap III-V semiconductors. Current developments of TPV systems are based on semiconductors with a cutoff wavelength range of 1.9 to 2.6 μm, and thermal sources that operate in the more moderate temperature range of 1100 to 1500 K [1]. There are several semiconductor materials systems that satisfy the energy gap requirement. For example, InGaAs grown on InP substrates has been pursued with some success. However, the alloy composition that satisfies this wavelength range is lattice mismatched to the InP substrate, and although defect-filtering schemes have been employed, the device performance is compromised by crystalline defects [2,3]. Similarly, InGaSb grown on GaSb substrates has shown some promise, but also is lattice mismatched [4].

Alternative low bandgap materials systems which can be lattice matched to binary substrates are GaInAsSb or InAsPSb. GaInAsSb is of particular interest for TPV's since these alloys have successfully been grown for detectors and lasers. Recently, we reported the highest performing TPV devices with a 2.3 μm cutoff wavelength, internal quantum efficiency of ~90%, and large open circuit voltage of ~300 meV [5]. The epitaxial structures, which are typically

~5 μm in thickness, were grown by both organometallic vapor phase epitaxy (OMVPE) and molecular beam epitaxy (MBE) and exhibited similar high performance. Since higher growth rates are attainable in OMVPE compared to MBE, OMVPE is especially attractive for preparation of TPV device structures.

In this paper, we review some of our recent work on OMVPE of $Ga_{1-x}In_xAs_ySb_{1-y}$ alloys with 2 to 2.4 μm cutoff wavelength [6], and report on new results. In particular, we have increased the growth rate from 2.5 to 5 μm/h, while also improving the overall quality of $Ga_{1-x}In_xAs_ySb_{1-y}$ lattice matched to GaSb. Furthermore, we have further extended room temperature photoluminescence (PL) emission to 2.5 μm. Low temperature PL spectra exhibit (full width at half-maximum) FWHM as narrow as 5 meV. We also report the device characteristics of recent TPV cells. The device results are remarkably consistent and exhibit near-theoretical performance limits.

2. The $Ga_{1-x}In_xAs_ySb_{1-y}$ quaternary alloy

The energy gap dependence on composition of the $Ga_{1-x}In_xAs_ySb_{1-y}$ quaternary alloy, based on the binary bandgaps [7], is given by $E(x,y) = 0.726 - 0.961x - 0.501y + 0.08xy + 0.415x^2 + 1.2y^2 + 0.021x^2y - 0.62xy^2$. Although this alloy has the advantage that it can be lattice matched to either GaSb or InAs substrates, growth on GaSb substrates is perferred over InAs because of thermodynamic considerations [8] and electronic band structure [9]. For alloys lattice matched to GaSb, $y = 0.867(x)/(1 - 0.048x)$. Figure 1 shows the energy gap dependence on As for various In concentrations for TPV's, and the unique alloy composition for lattice matching to GaSb at room temperature. The energy gap is determined in large part by the In content of the alloy, while the As content mainly affects the lattice constant.

Alloys grown lattice matched to GaSb substrates have energy gap that is adjustable in the wavelength range of 1.7 to 4.2 μm. However, most of the alloy compositions are thermodynamically unstable [8]. Even so, $Ga_{1-x}In_xAs_ySb_{1-y}$, alloys near or within the

miscibility gap have been successfully grown by a number of epitaxial techniques which include liquid phase epitaxy (LPE) [10], OMVPE [6,8,11-13], and MBE [14,15].

3. Epitaxial growth and characterization

$Ga_{1-x}In_xAs_ySb_{1-y}$ epilayers were grown in a vertical rotating-disk reactor with H_2 carrier gas at a flow rate of 10 slpm, reactor pressure of 150 Torr, and a typical rotation rate of 100 rpm [6]. Solution trimethylindium (TMIn), triethylgallium (TEGa), tertiarybutylarsine (TBAs), and trimethylantimony (TMSb) were used as organometallic precursors. The selection of these sources was based on several criteria. Since $Ga_{1-x}In_xAs_ySb_{1-y}$ alloys have a low melting point, the precursors should have a low thermal decomposition temperature for mass-transport limited growth. Therefore, TEGa and TBAs are preferred over trimethlylgallium and arsine, respectively, whose pyrolysis temperatures are over 100 °C higher than their counterparts. We selected TMSb over triethylantimony (TESb) in spite of the higher pyrolysis temperature of TMSb because previous studies of GaSb growth from TEGa and TESb suggested source prereactions with TESb, but not with TMSb [16]. (All sources are premixed in a single fast-switching manifold before introduction into the reactor.) TMIn and TEGa were maintained at 24°C, TMSb at 0°C, and TBAs at -8°C. For doping studies, diethyltellurium (DETe) (10 ppm in H_2) and dimethylzinc (DMZn) (1000 ppm in H_2) were used as n- and p-type doping sources, respectively.

The total group III mole fraction ranged from 1.7 to 7.6 x 10^{-4}, which resulted in a growth rate of ~1.5 to 5 μm/h. The TMIn fraction in the gas phase, $p_{TMIn}/[p_{TMIn} + p_{TEGa}]$, was varied from 0.09 to 0.27 and the V/III ratio from 0.9 to 1.7. For lattice matching to GaSb substrates, the TBAs fraction in the gas phase, $p_{TBAs}/[p_{TBAs} + p_{TMSb}]$, was varied from 0.05 to 0.2. Epilayers were grown at 525, 550, and 575°C.

$Ga_{1-x}In_xAs_ySb_{1-y}$ epilayers were grown without a GaSb buffer on (100) Te-doped GaSb substrates misoriented 2° toward (110) or 6° toward (111)B. For electrical characterization, semi-insulating (SI) GaAs substrates of similar orientations were used because SI GaSb

substrates are not available. Just before loading the GaSb and GaAs substrates into the reactor, they were degreased in solvents and acid etched. GaAs substrates were etched for 30 s in 5:1:1 H_2SO_4:H_2O_2:H_2O, and rinsed in deionized water. GaSb substrates were first etched in concentrated HCl for 3 min, followed by a 1 min etch in Br_2-HCl-HNO_3-CH_3COOH, and rinsed in isopropanol. This etch yielded excellent and reproducible GaSb surfaces for epitaxy, provided that the etch solution was freshly mixed.

The surface morphology was examined using Nomarski contrast microscopy. Double-crystal x-ray diffraction (DCXD) was used to measure the degree of lattice mismatch ($\Delta a/a$) to GaSb substrates. PL was measured at 4 and 300K using a PbS detector. The In and As content of epilayers was determined from DCXD splitting, the peak emission in 300 K PL spectra, and the energy gap dependence on composition based on the binary energy gaps. For electrical characterization, GaInAsSb was grown at 525 or 550°C on SI (100) GaAs substrates. Since the mismatch between GaInAsSb and GaAs is ~8%, a GaSb buffer layer, typically 0.4 μm thick, was first grown at 550°C to reduce the contribution of electrically active defects due to the lattice mismatch [6]. Carrier concentration and mobility of GaInAsSb epilayers, which were grown about 3 μm thick, were obtained from Hall measurements based on the van der Pauw method.

4. Growth results

4.1 Alloy composition control

As discussed above, the energy gap of $Ga_{1-x}In_xAs_ySb_{1-y}$ is affected primarily by the x-value, while the y-value is used to adjust the lattice constant to match to the GaSb substrate. The distribution coefficients of In and As are summarized in Figs. 2a and 2b, respectively. The growth temperature was 525, 550, or 575°C; the growth rate ranged from 1.5 to 5 μm/h; and the V/III ratio ranged between 1.1 and 1.4. Test data include those previously reported [6] as well as new data for layers grown on both (100) 2° toward (110) and (100) 6° toward (111)B substrates, for layers grown at the higher growth rate of 5 μm/h, and for layers grown at 525°C. For all

layers, $|\Delta a/a| < 2 \times 10^{-3}$. At 525°C, the In distribution coefficient is 1.2, and decreases to 0.95 and 0.5 at 550 and 575°C, respectively. The trend of a lower In distribution coefficient with increasing temperature is similar to results reported for growth using TMGa and TMIn [8,17]. However, in those studies, the dependence is attributed to the increase in TMGa pyrolysis with temperature. For the range of growth temperatures and reactor used in this study, it is likely that both TMIn and TEGa are completely pyrolyzed. Thus, these results may reflect a difference in In-related surface kinetics. Figure 2b shows that the As distribution coefficient is approximately unity independent of growth temperature, indicating complete pyrolysis of TBAs and TMSb. In contrast, the As distribution coefficient was reported to be a strong function of temperature when TMGa, TMIn, TBAs, and TMSb were used as precursors [17].

The degree of lattice mismatch of $Ga_{1-x}In_xAs_ySb_{1-y}$ epilayers on GaSb can influence the performance of minority carrier type. Therefore, we determined the sensitivity of lattice mismatch on the fraction of TBAs in the gas phase. Figure 3 shows the lattice mismatch as a function of TBAs fraction in the gas phase for various TMIn fractions and total group III mole fractions. On average, the sensitivity is about 2×10^{-3} % per TBAs fraction in the gas phase, and is independent of growth temperature and growth rate.

4.2 Structural properties

As reported previously [6], the surface morphology of $Ga_{1-x}In_xAs_ySb_{1-y}$ layers depends on V/III ratio, substrate misorientation, In content, and growth temperature. Below a critical V/III ratio, which is slightly higher than 1 for the growth temperature range in this study, the $Ga_{1-x}In_xAs_ySb_{1-y}$ is metal-rich and the surface is hazy to the naked eye. However, a surface texture, as observed by Nomarski contrast microscopy, developed when the V/III ratio was increased just above the minimum V/III ratio. The surface morphology of epilayers grown on (100) 2° toward (110) substrates is more sensitive to growth conditions than (100) 6° toward (111)B substrates, and a smoother surface morphology is observed for layers grown on substrates with a 6° toward (111)B misorientation.

The In content also affects the surface morphology. Figure 4 shows the surface morphology of $Ga_{1-x}In_xAs_ySb_{1-y}$ layers with various In concentrations. These layers were grown at 525 °C with a growth rate of 5 μm/h on (100) 6° toward (111)B GaSb substrates. As the In concentration increases, the surface morphology exhibits increased texture. The degradation in surface morphology is likely related to the increased instability of the alloy since the composition corresponds to regions further in the miscibility region [8]. The surface morphology of $Ga_{1-x}In_xAs_ySb_{1-y}$ grown under similar conditions on (100) 2° toward (110) substrates (Fig. 5), however, exhibited facetted defects.

The DCXD of nominally lattice matched $Ga_{1-x}In_xAs_ySb_{1-y}$ epilayers also exhibited a dependence on the In concentration. Figure 6 shows DXCD scans for epilayers about 2 μm in thickness. The full width at half-maximum (FWHM) of the epilayer peak is comparable to that of the GaSb substrate for In = 0.09 (Fig. 6a). It increases with increasing In, and for In ~ 0.20 (Fig. 6c), the layer peak is extremely broadened. This broadening may be the precursor to phase separation of the $Ga_{1-x}In_xAs_ySb_{1-y}$ metastable alloy.

4.3 Optical properties

Figure 7 shows the 4 and 300 K PL spectra for $Ga_{1-x}In_xAs_ySb_{1-y}$ layers of two different compositions grown at 525°C on (100) GaSb substrates with a 6° toward (111)B misorientation. The layers are ~2 μm in thickness, and the growth rate was 5 μm/h. The peak emission for the sample shown in Fig. 7a (x = 0.16, y = 0.15) is 2080 nm at 4 K and 2320 nm at 300 K. The 4 K FWHM is 7.5 meV. For the sample shown in Fig. 7b (x = 0.2, y = 0.18), the peak emission is 2225 nm at 4 K and 2505 nm at 300 K. The FWHM at 4 K increases to 25 meV which is not surprising since this alloy penetrates further into the miscibility gap. Although lattice matched $Ga_{1-x}In_xAs_ySb_{1-y}$ layers of higher In composition (see Fig. 4d) could be grown, this layer did not exhibit PL at 4 or 300 K. The longest PL emission at 300 K observed in our current study is 2525 nm.

Figure 8 summarizes our best FWHM data for $Ga_{1-x}In_xAs_ySb_{1-y}$ epilayers, which shows improvement over our previous results [6]. These layers were grown at 525 or 550°C, and at various growth rates. Several trends are observed. The PL FWHM values are strongly dependent on growth temperature and peak energy, and weakly dependent on growth rate. The lowest PL FWHM values are obtained for layers grown at the lower temperature of 525°C. The narrowest PL FWHM values are ~5 meV for 4 K peak energy greater than 0.62 eV, and increase sharply below 0.60 eV. A slight improvement in FWHM values are observed for layers grown at the higher growth rates. Since broadening in PL spectra can be a result of alloy scattering [18], the data suggest increased alloy clustering especially for layers with composition approaching the miscibility gap [8]. Our FWHM values are significantly smaller than those reported previously for OMVPE-grown layers [8,12,17], especially for those layers with lower PL peak energy. The smallest FWHM value measured is 4.7 meV at 0.643 eV. Our FWHM values are favorably comparable to those reported for layers grown by MBE [11] and by LPE [19].

For GaInAsSb alloys, PL results are usually reported at low temperature. The emission at room temperature is then estimated from these low temperature results and an interpolation based on the energy difference of the 4 and 300 K near-bandedge transitions for GaSb [20] and InAs [21]. However, our results shown in Fig. 9 indicate that such extrapolations can be in error. The energy difference between the 4 and 300 K PL is plotted as a function of the 4 K PL peak energy for GaInAsSb alloys grown at 525, 550, and 575°C. For most of the GaInAsSb alloys grown at 525 or 550°C, this energy difference ranges between 0.05 and 0.07 meV, which is in line with the difference for GaSb and InAs binaries. However, for alloys grown at 575°C, the 4 and 300 K energy difference decreases from about 65 to 10 meV as the 4 K PL peak energy decreases to 0.6 eV. The FWHM values also increased to about 20 to 30 meV, which suggests that the 4 K PL emission may be related to impurity or defect transitions.

4.4 Electrical properties

The carrier concentration and mobility were measured from GaInAsSb layers grown on SI GaAs substrates because SI GaSb substrates are not available. Since the lattice mismatch between GaInAsSb (lattice matched to GaSb) and GaAs is 8%, a 0.4-μm-thick GaSb buffer was first grown at 550°C as described previously [6], followed by the GaInAsSb epilayer. Nominally undoped GaInAsSb layers are p-type. The lowest residual hole concentration and highest mobility values were measured for layers grown at 550°C. The typical hole concentration is as low as 5×10^{15} cm^{-3} with a corresponding mobility of 430 $cm^2/V\text{-}s$. Considerably higher hole concentration (2 to 5×10^{16} cm^{-3}) and lower mobility (220 to 320 $cm^2/V\text{-}s$) were recently reported for GaInAsSb grown with TMGa, TMIn, arsine, and TMSb [22]. For GaInAsSb layers grown by MBE, the hole concentration was reported to be 4 to 5×10^{16} cm^{-3} and the mobility to be 254 $cm^2/V\text{-}s$ [23].

The 300 K electrical properties of p- and n-doped $Ga_{1-x}In_xAs_ySb_{1-y}$ (x~0.13, y~0.12) grown at 525 and 550°C are summarized in Figs. 10a and 10b, respectively. The plots include data from layers grown at a rate of either 2.5 or 5 μm/h. Because the electrical characteristics are similar for layers grown on (100) 2° toward (110) and on (100) 6° toward (111)B (not differentiated in Figs. 10a and 10b), the compensation mechanism is similar. Data plotted are for GaInAsSb grown on a 0.4- and 0.8-μm-thick buffer layers. The hole concentration ranges from 4.4×10^{15} to 1.8×10^{18} cm^{-3} with mobility values between 560 and 180 $cm^2/V\text{-}s$, respectively. The electron concentration ranges from 2.3×10^{17} to 4.2×10^{18} cm^{-3}, with corresponding mobility values between 5208 and 2084 $cm^2/V\text{-}s$, respectively. These mobility values are likely to be an underestimate of true values, since the mismatch is significant, and the procedure for the GaSb buffer layer growth has not been optimized. Although there is extremely limited data for GaInAsSb electrical properties, we believe these results are a significant improvement over results reported previously [12,22,23].

5. Thermophotovoltaic Devices

TPV device structures were grown on (100) GaSb substrates with either 2° toward (110) or 6° toward (111)B misorientation. The growth temperature was 525 or 550°C. The TPV structure consists of the following layers: 0.4-μm-thick n-GaSb buffer layer, 1-μm-thick n-GaInAsSb base layer (doped to 5 x 10^{17} cm^{-3}), 3- to 5-μm-thick p-GaInAsSb emitter layer (doped to 2 x 10^{17} cm^{-3}), 0.1-μm-thick p-AlGaAsSb window layer (doped to 4 x 10^{17} cm^{-3}), and 0.05-μm-thick p-GaSb contact layer (doped to 2 x 10^{18} cm^{-3}), grown on a GaSb substrate. In some cases, the AlGaAsSb window layer was omitted, and a p-GaSb layer was grown as both window and contact layer.

Large-area (1 cm^2) TPV cells were fabricated by a conventional photolithographic process. A single 1-mm-wide central busbar connected to 10-μm-wide grid lines spaced 100 μm apart was used to make electrical contact to the front surface. Ohmic contacts to p- and n-GaSb were formed by depositing Ti/Pt/Au and Au/Sn/Ti/Pt/Au, respectively, and alloying at 300°C. Mesas were formed by wet chemical etching to a depth of ~5 μm. No antireflection coatings were deposited on these test devices.

The external quantum efficiency (QE) of several representative TPV devices is plotted as a function of wavelength in Fig. 11. The QE is typically between 55 and 60% and has a cutoff wavelength of 2.3 μm. The highest QE measured is 70%, which is approaching the 100% internal quantum efficiency limit if a surface reflection of 30% is assumed. The open circuit voltage (V_{oc}) as a function of short circuit current density (J_{sc}) is shown in Fig. 12. At 1 A/cm^2, V_{oc} is a high value of 300 meV. The fill factor for these devices is typically 69%. Over the course of several months, we have grown and fabricated nearly 40 TPV wafers. The average external QE is 59.3% with a standard deviation of 3.8%, and only one device with external QE less than 50% was measured.

6. Conclusions

High quality GaInAsSb epilayers were grown lattice matched to GaSb substrates by OMVPE using TEGa, TMIn, TBAs, and TMSb at 525, 550, and 575°C. Mirror-smooth surface morphology was obtained for alloys with 300 K PL emission in the wavelength range 2 to 2.5 μm. In general, the highest material quality is observed for layers grown at the lowest temperature 525°C, and on (100) 6° toward (111)B GaSb substrates. Layer quality also shows improvement when the growth rate is increased from 2.5 to 5 μm/h. TPV devices exhibit both high internal quantum efficiency and high V_{oc}. This work demonstrates that the OMVPE growth technology is extremely attractive for the synthesis of GaInAsSb materials for TPV devices.

Acknowledgments

The authors gratefully acknowledge D.R. Calawa for x-ray diffraction, J.W. Chludzinski for photoluminescence, P.M. Nitishin for technical assistance in characterization, K.J. Challberg for manuscript editing, and D.L. Spears for continued support and encouragement.

References

1. 2nd NREL Conference on the Thermophotovoltaic Generation of Electricity, edited by J.P. Benner, T.J. Coutts, and D.S. Ginley, AIP Conference Proceedings Vol. 358, Woodbury, NY, 1995.

2. M.W. Wanlass, J.S. Ward, K.A. Emery, M.M. Al-Jassim, K.M. Jones, and T.J. Coutts, Solar Energy Mater. Solar Cells 44/42 (1996) 405.

3. S. Wojtczuk, P. Colter, G. Charache, and B. Campbell, Proc. 25th IEEE Photovoltaic Specialist Conf. (1996) 77.

4. H. Ehsani, I. Bhat, C. Hitchcock, R. Gutman, G. Charache, and M. Freeman, in 3nd NREL Conference on the Thermophotovoltaic Generation of Electricity, edited by T.J. Coutts, C.S. Allman, and J.P. Benner, AIP Conference Proceedings Vol. 401, Woodbury, NY, 1997, p. 65.

5. H.K. Choi, C.A. Wang, G.W. Turner, M.J. Manfra, D.L. Spears, G.W. Charache, L.R. Danielson, and D.M. Depoy, Appl. Phys. Lett. 71 (1997) 3758.

6. C.A. Wang, accepted J. Cryst. Growth.

7. J.C. DeWinter, M.A. Pollock, A.K. Srivastava, and J.L. Zyskind, J. Electron. Mater. 14 (1985) 729.

8. M.J. Cherng, H.R. Jen, C.A. Larsen, G.B. Stringfellow, H. Lundt, and P.C. Taylor, J. Cryst. Growth 77 (1986) 408.

9. A.G. Milnes and A.Y. Polyakov, Mater. Sci. Eng. B18 (1993) 237.

10. E. Tournie, F. Pitard, and A. Joullie, J. Cryst. Growth 104 (1990) 683.

11. C.A. Wang, H.K. Choi, G.W. Turner, D.L. Spears, M.J. Manfra, and G.W. Charache, in 3rd NREL Conference on the Thermophotovoltaic Generation of Electricity, edited by J.P. Benner and T.J. Coutts, AIP Conference Proceedings Vol. 401, Woodbury, NY, 1997, p. 75.

12. J. Shin, T.C. Hsu, Y. Hsu, and G.B. Stringfellow, J. Cryst. Growth 179 (1997) 1.

13. A. Giani, J. Bougnot, F. Pascal-Delannoy, G. Bougnot, J. Kaoukab, G.G. Allogho, and M. Bow, Mater. Sci. Eng. B 9 (1991) 121.

14. H.K. Choi, S.J. Eglash, and G.W. Turner, Appl. Phys. Lett. 64 (1994) 2474.

15. T.H. Chui, J.L. Zyskind, and W.T. Tsang, J. Electron. Mater. 16 (1987) 57.

16. C.A. Wang, S. Salim, K.F. Jensen, and A.C. Jones, J. Cryst. Growth 170 (1997) 55.

17. M. Sopanen, T. Koljonen, H. Lipsanen, and T. Tuomi, J. Cryst. Growth 145 (1994) 492.

18. J. Singh and K.K. Bajaj, Appl. Phys. Lett. 44 (1984) 1075.

19. E. Tournie, J.-L. Lazzari, F. Pitard, C. Alibert, A. Joullie, and B. Lambert, J. Appl. Phys. 68 (1990) 5936.

20. S.C. Chen and Y.K. Su, J. Appl. Phys. 66 (1989) 350.

21. Z.M. Fang, K.Y. Ma, D.H. Jaw, R.M. Cohen, and G.B. Stringfellow, J. Appl. Phys. 67 (1990) 7034.

22. A. Giani, F. Pascal-Delannoy, J. Podlecki, and G. Bougnot, Mater. Sci. Eng. B 41 (1996) 201.

23. A.Z. Li, J.Q. Zhong, Y.L. Zheng, J.X. Wang, G.P. Ru, W.G. Bi, and M. Qi, J. Cryst. Growth 150 (1995) 1375.

Figure Captions

Figure 1 300 K energy gap dependence of $Ga_{1-x}In_xAs_ySb_{1-y}$ as a function of As for various In compositions.

Figure 2 Distribution coefficients of (a) In and (b) As for $Ga_{1-x}In_xAs_ySb_{1-y}$ epilayers grown nominally lattice matched to GaSb at 525°C (open squares), 550°C (solid circles), and 575°C (open circles).

Figure 3 Lattice mismatch as a function of TBAs fraction in the gas phase for $Ga_{1-x}In_xAs_ySb_{1-y}$ epilayers grown at 525°C. TMIn fraction ranges from 0.09 to 0.21.

Figure 4 Surface morphology of nominally lattice matched $Ga_{1-x}In_xAs_ySb_{1-y}$ epilayers grown at 525°C on (100) 6° toward (111)B GaSb substrates with compositions: (a) $x = 0.09$, $y = 0.08$; (b) $x = 0.16$, $y = 0.15$; (c) $x = 0.20$, $y = 0.18$; (d) $x \sim 0.23$, $y \sim 0.21$ The composition for the layer shown in (d) is estimated from Fig. 2, since no room temperature photoluminescence was observed from the epilayer.

Figure 5 Surface morphology of $Ga_{1-x}In_xAs_ySb_{1-y}$ epilayers grown at 525°C on (100) 2° toward (110) GaSb.

Figure 6 Double crystal x-ray diffraction of $Ga_{1-x}In_xAs_ySb_{1-y}$ epilayers grown at 525°C on (100) 6° toward (111)B GaSb substrates with In compositions: (a) $x = 0.09$, $y = 0.08$; (b) $x = 0.16$, $y = 0.15$; (c) $x = 0.20$, $y = 0.18$.

Figure 7 Photoluminescence spectra measured at 4 and 300 K of $Ga_{1-x}In_xAs_ySb_{1-y}$ grown on (100) 6° toward (111)B GaSb substrates. Layers were grown at 525°C: (a) $x = 0.16$, $y = 0.15$; (b) $x = 0.20$, $y = 0.18$.

Figure 8 Photoluminescence full width at half-maximum measured at 4 K of GaInAsSb layers grown on GaSb substrates at 525°C (open squares), 550°C (solid circles), and 575°C (open circles).

Figure 9 Difference between 4 and 300 K photoluminescence peak energy as a function of 4 K peak energy. Layers were grown at 525°C (open squares), 550°C (solid circles), and 575°C (open circles).

Figure 10 Electrical properties measured at 300 K of (a) p-$Ga_{0.87}In_{0.13}As_{0.12}Sb_{0.88}$ and (b) n-$Ga_{0.87}In_{0.13}As_{0.12}Sb_{0.88}$. Closed circles represent data with 0.4-μm-thick GaSb buffer layer. Open circle for 0.8-μm-thick buffer layer.

Figure 11 External quantum efficiency of several TPV devices as a function of wavelength.

Figure 12 Open circuit voltage as a function of short circuit current density.

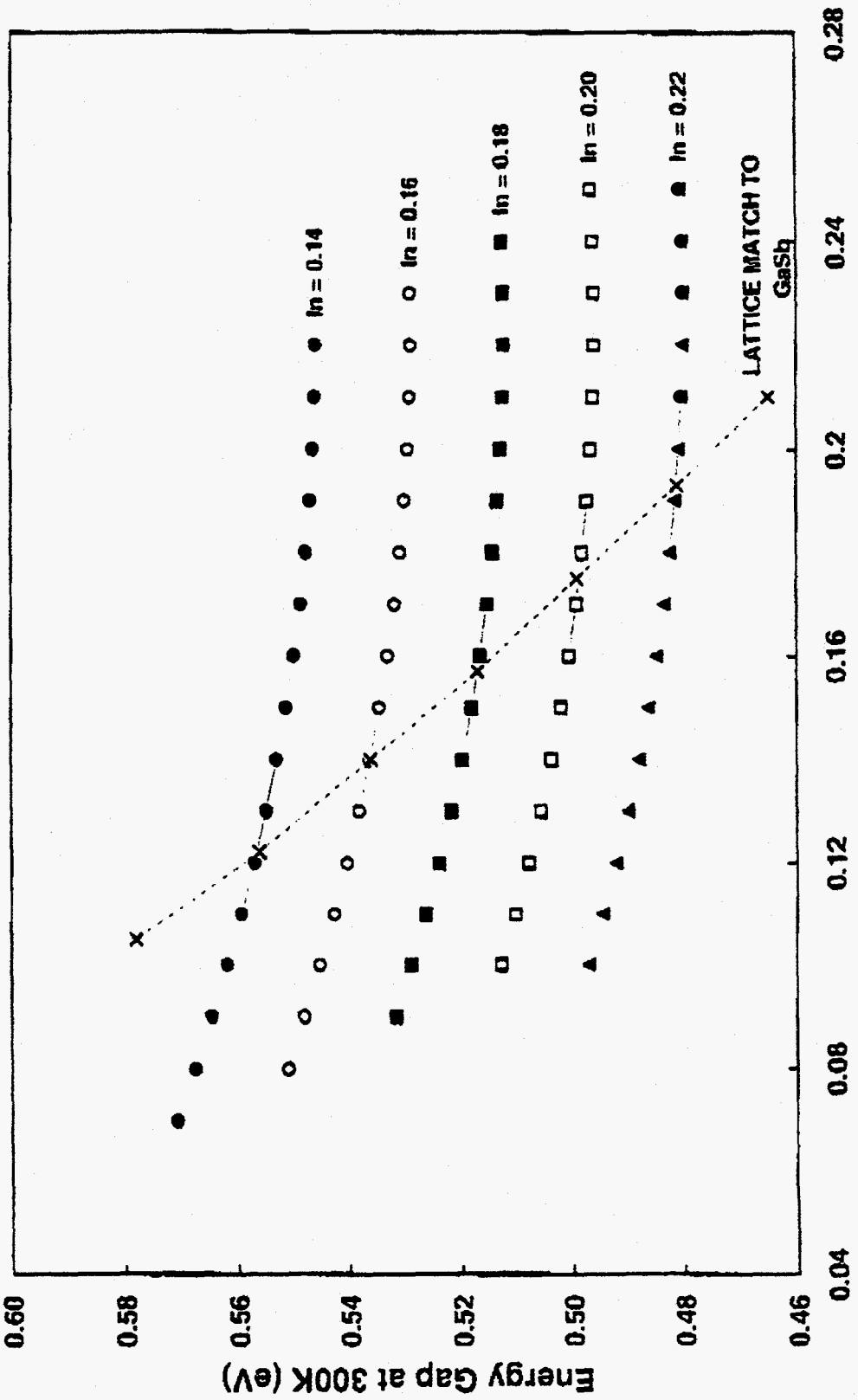
Energy Gap at 300K (eV)
0.60
0.58
0.56
0.54
0.52
0.50
0.48
0.46
0.04
0.08
0.12
0.16
0.2
0.24
0.28
As in GaInAsSb
In = 0.14
In = 0.16
In = 0.18
In = 0.20
In = 0.22
LATTICE MATCH TO GaSb

Figure 1

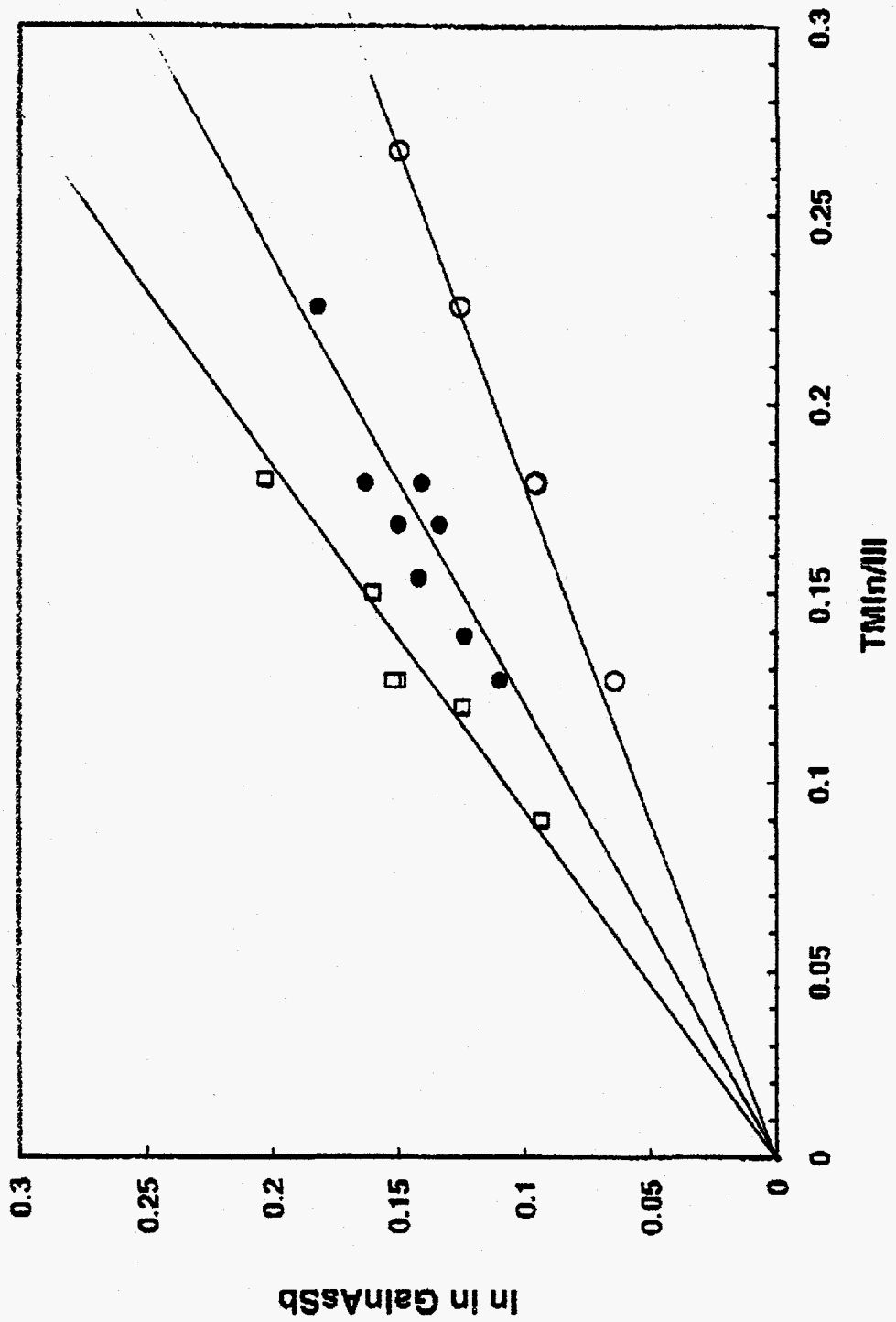

Figure 2a

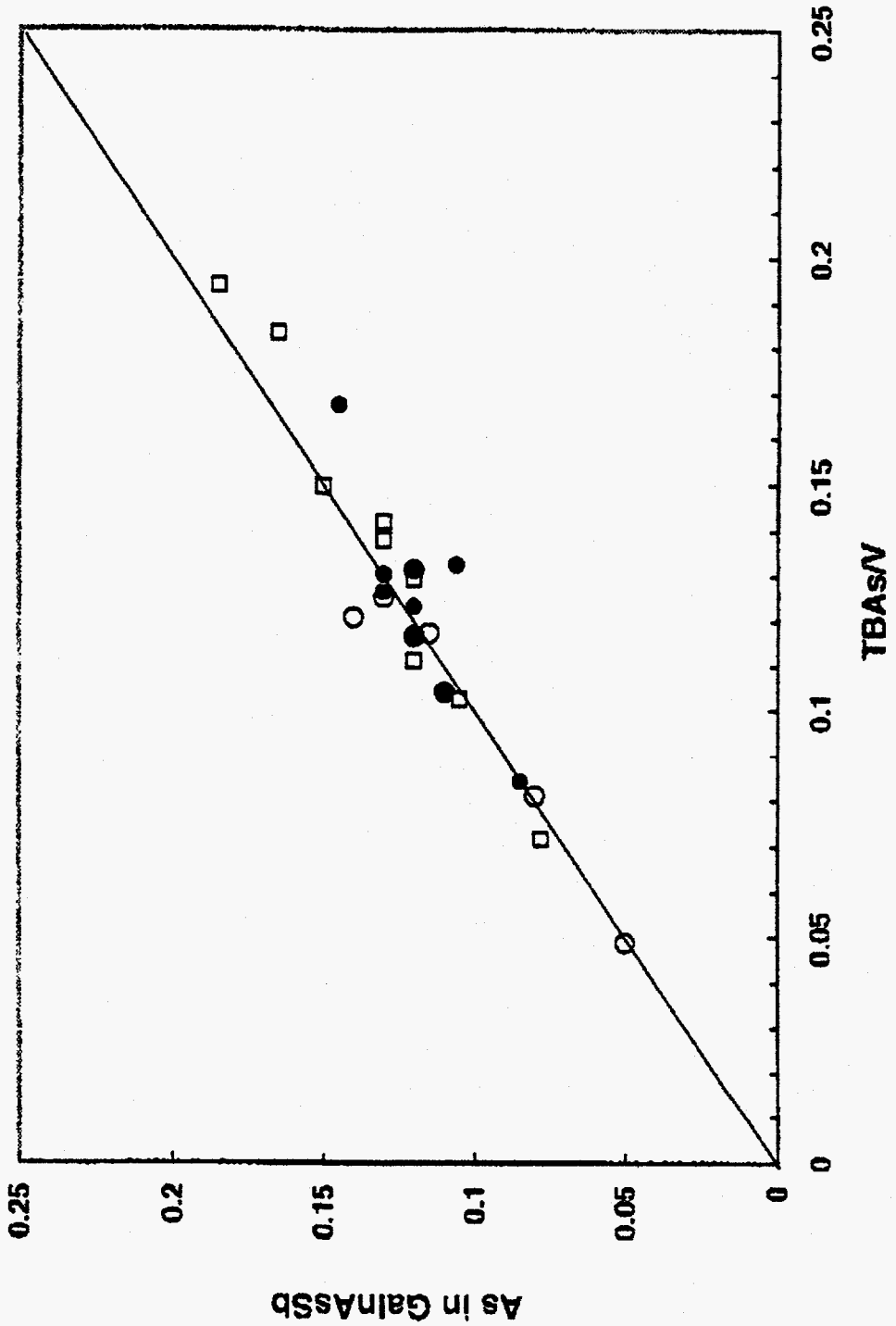

Figure 2b

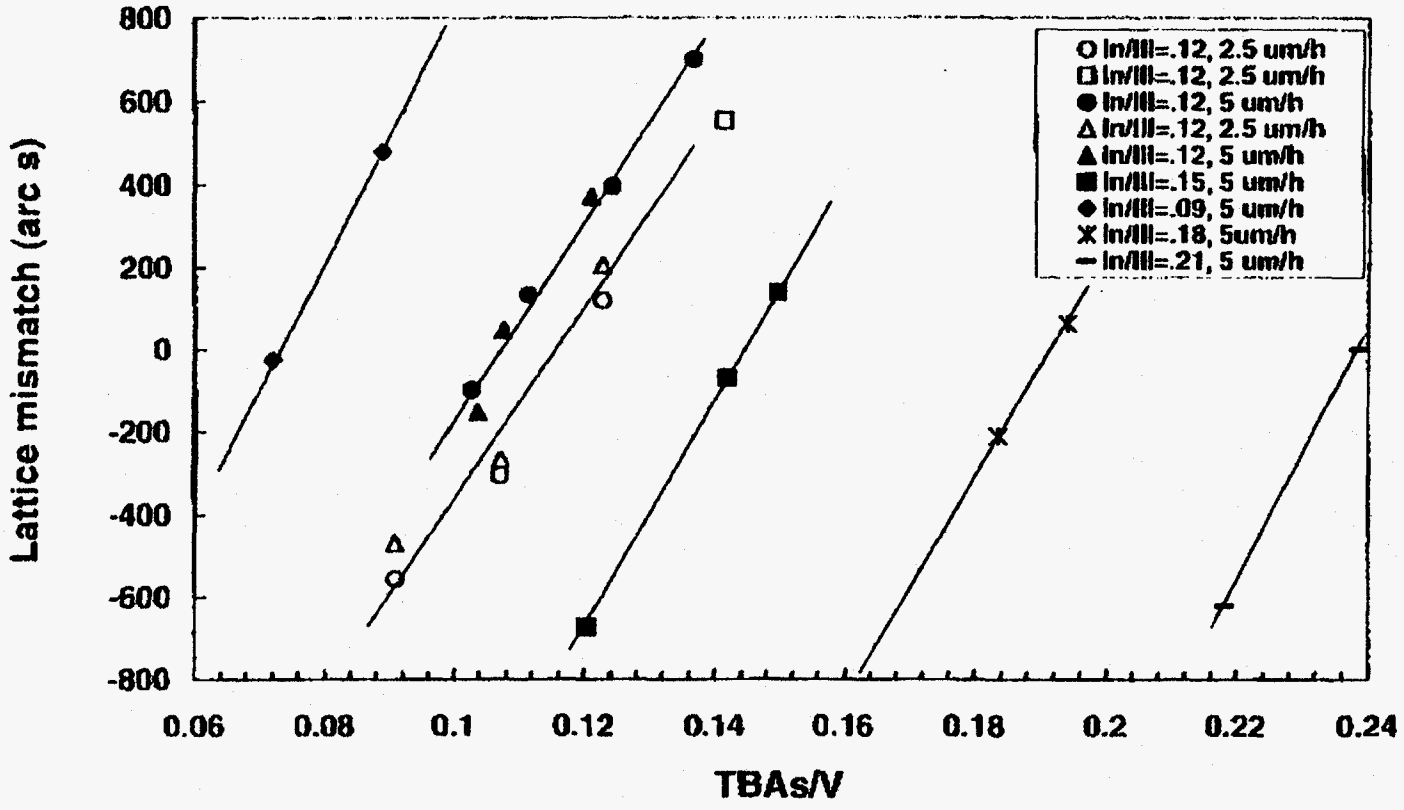

Figure 3

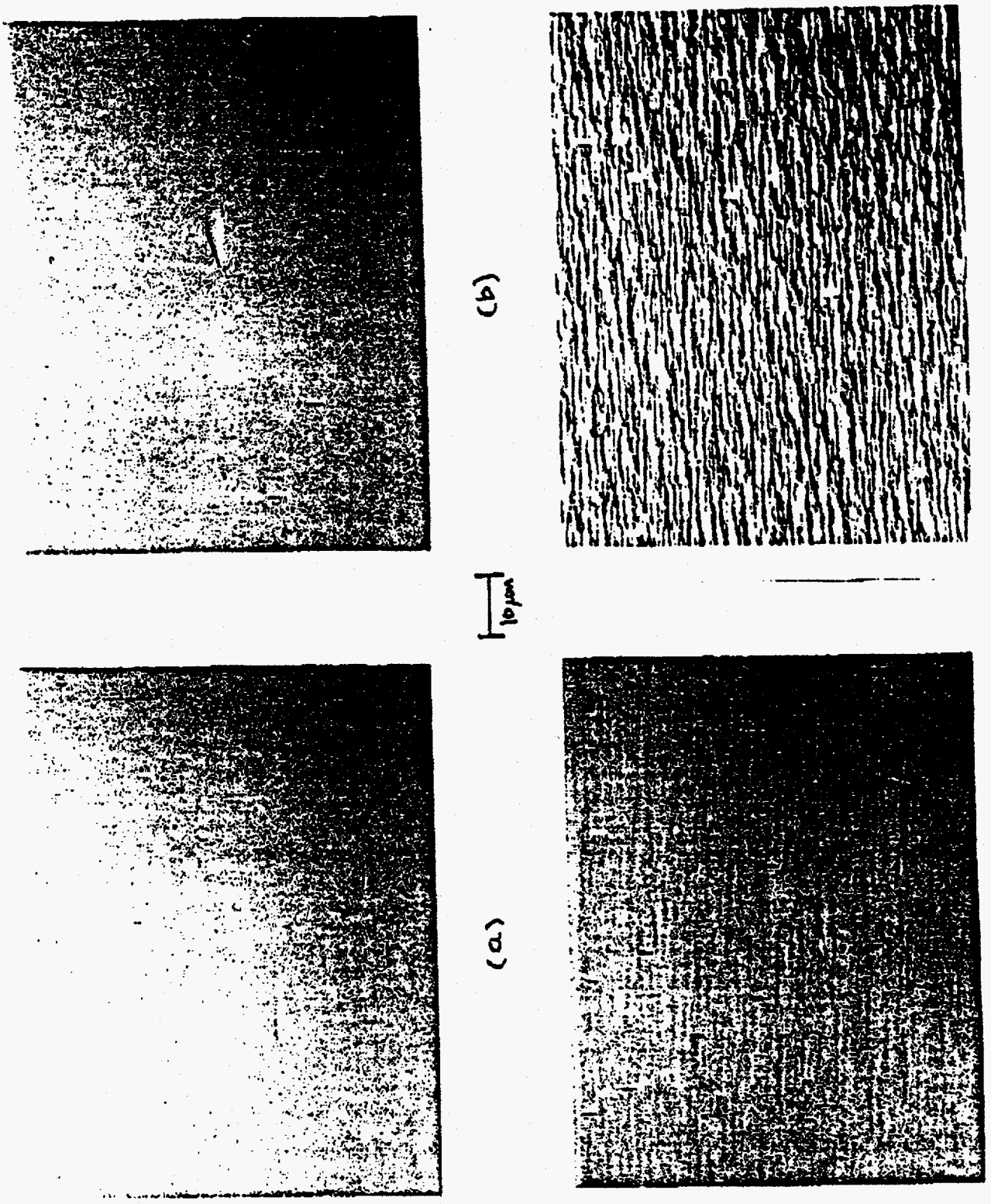

Figure 4

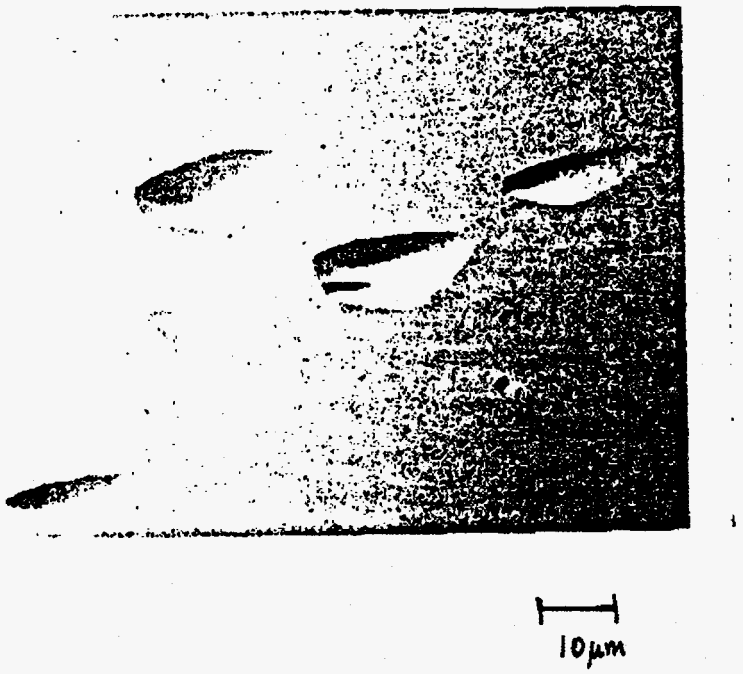

Figure 5

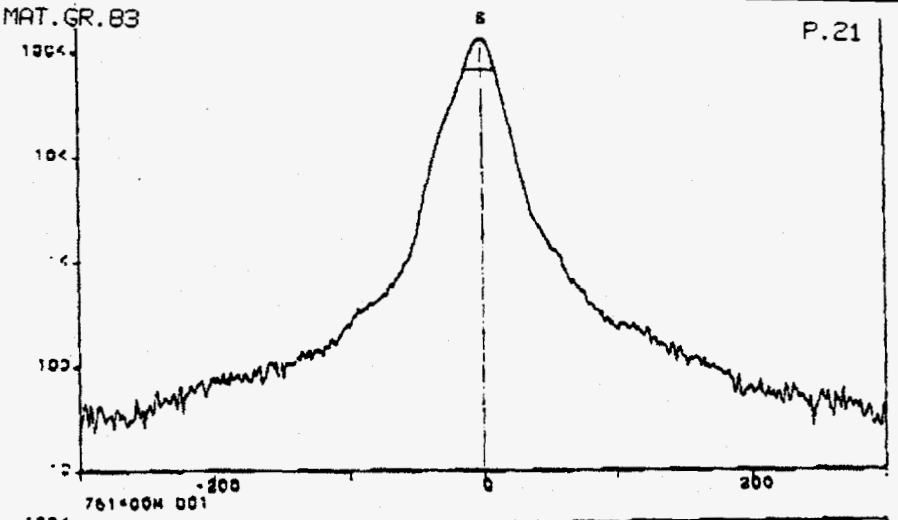

Figure 6a

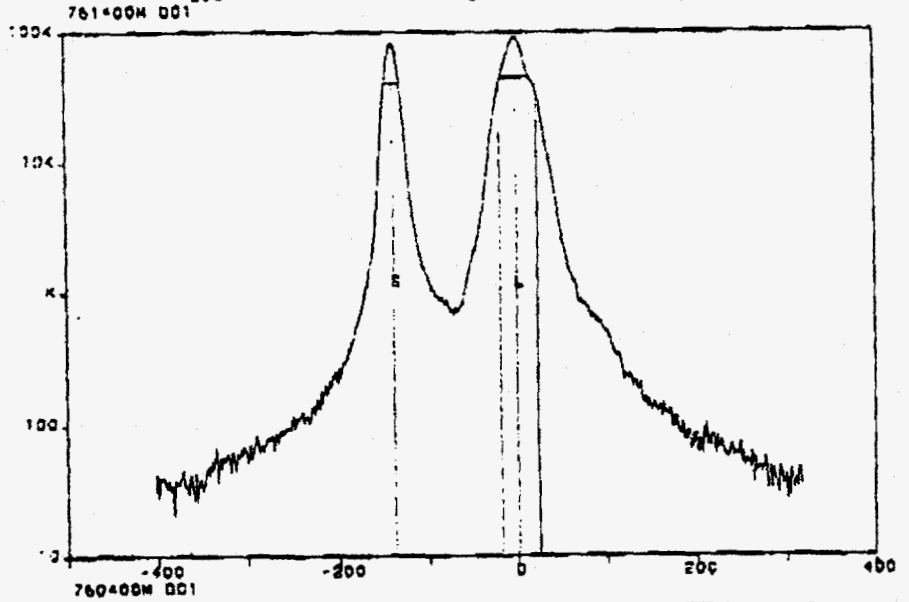

Figure 6b

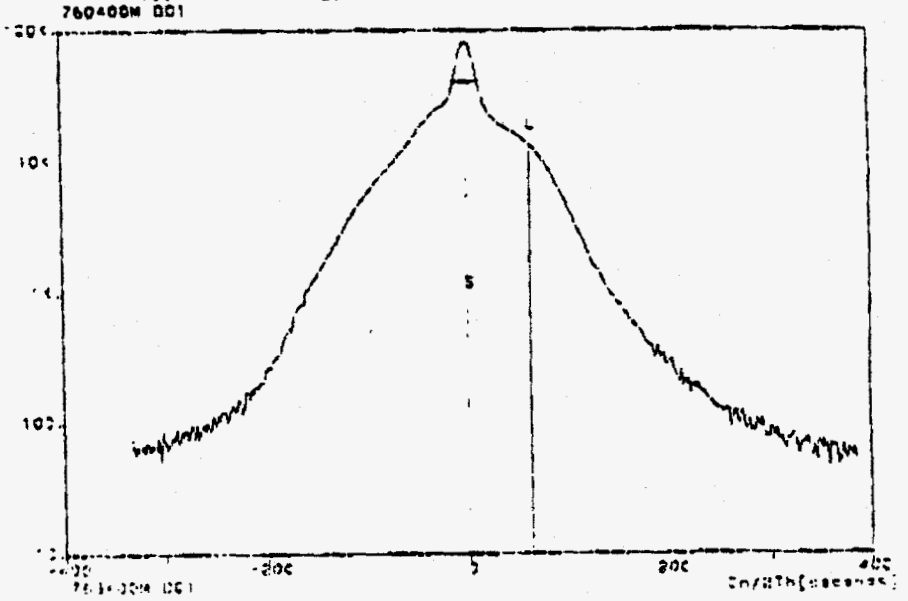

Figure 6c

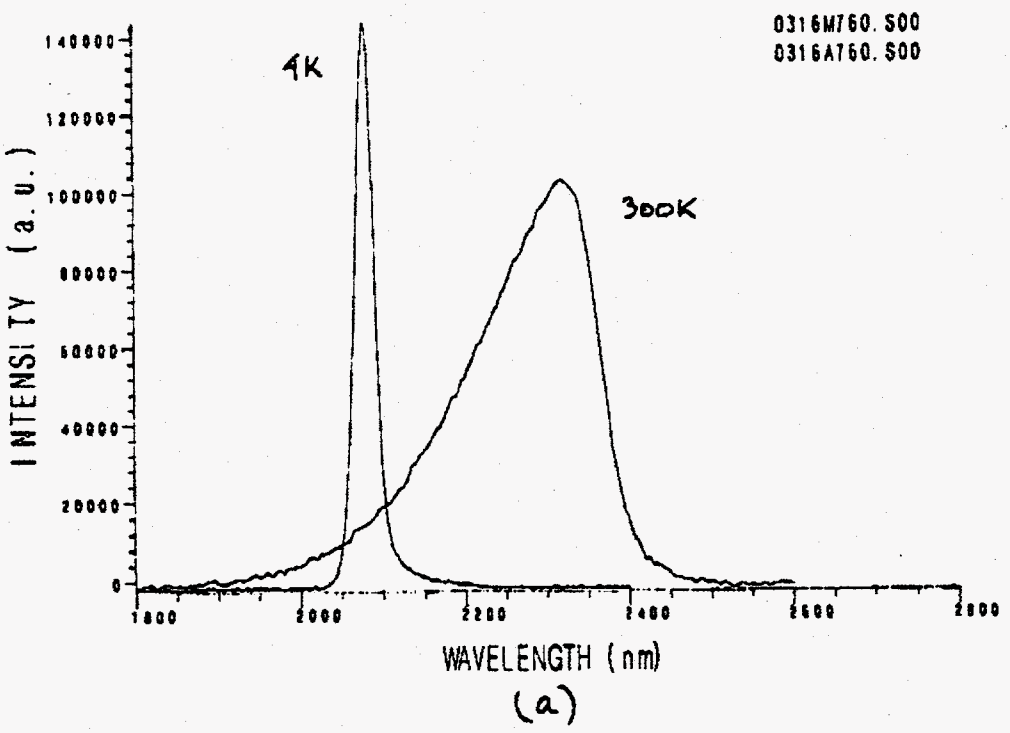
0316M760.S00
0316A760.S00
4K
300K
INTENSITY (a.u.)
WAVELENGTH (nm)

(a)

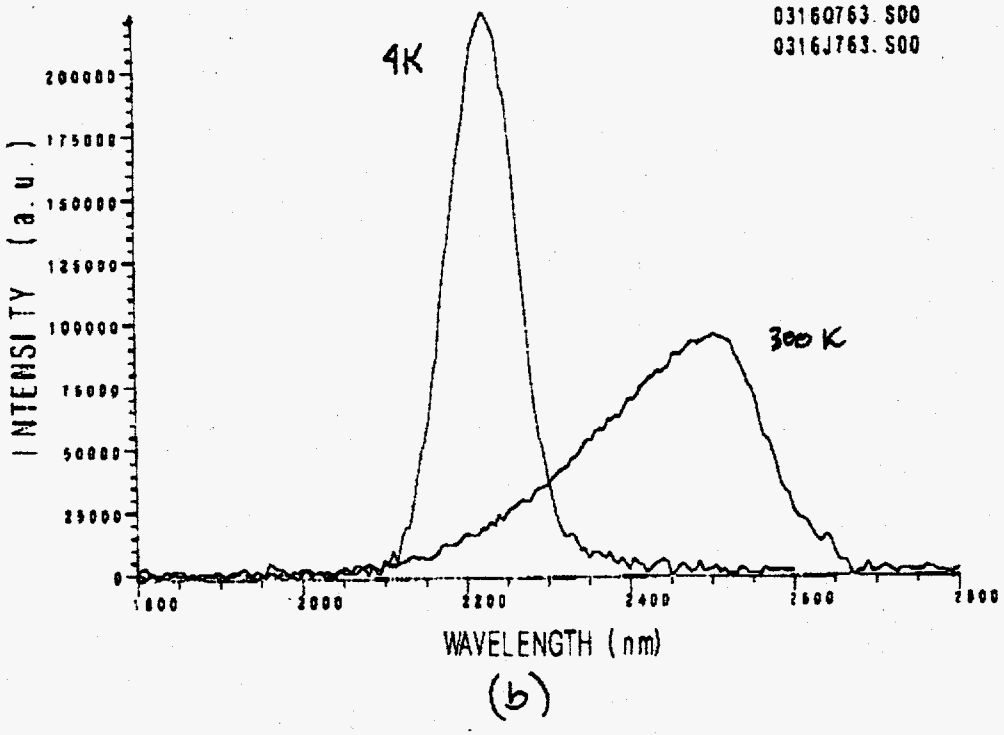
0316Q763.S00
0316J763.S00
4K
300 K
INTENSITY (a.u.)
WAVELENGTH (nm)

(b)

Figure 7

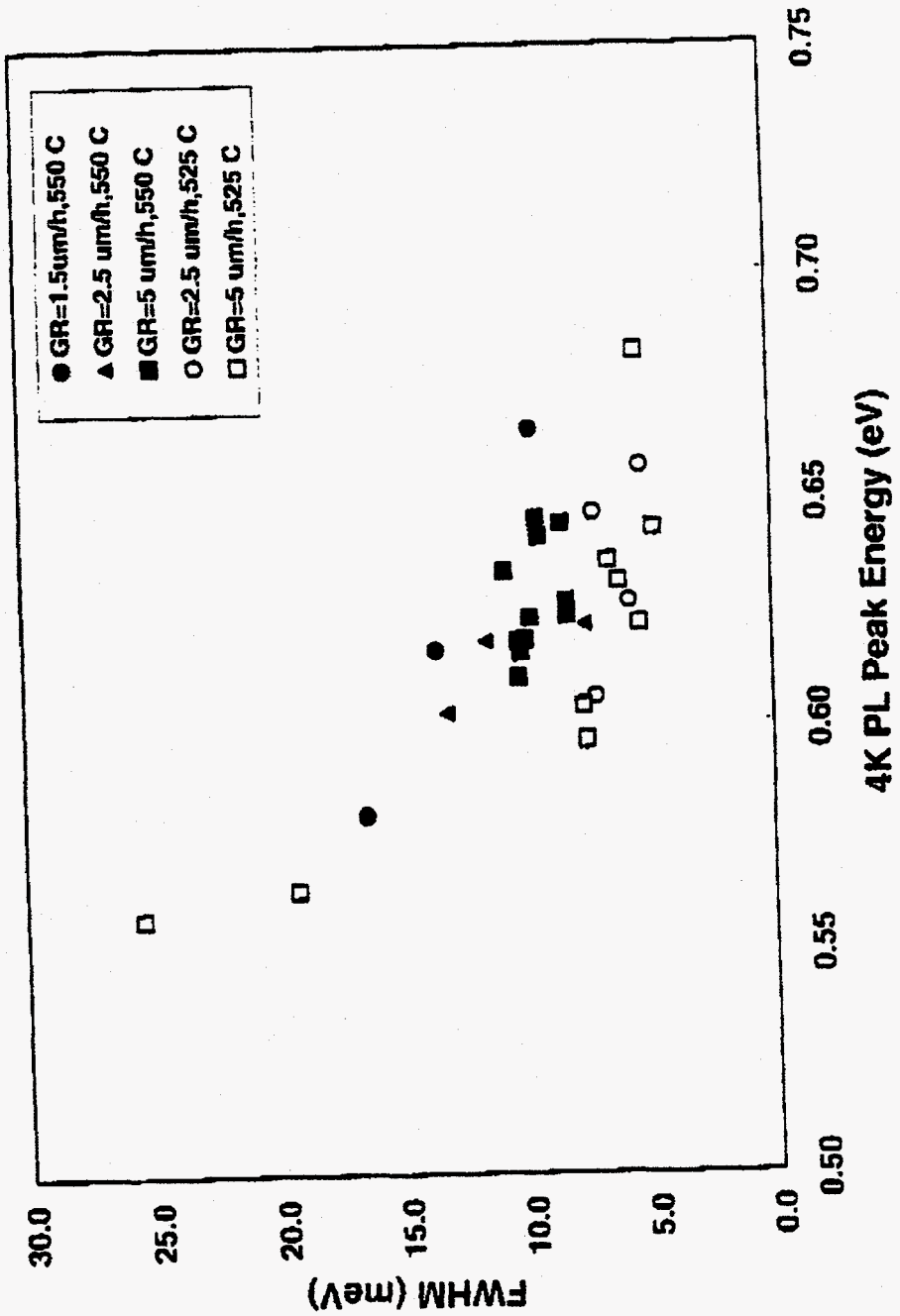
GR=1.5um/h,550 C
GR=2.5 um/h,550 C
GR=5 um/h,550 C
GR=2.5 um/h,525 C
GR=5 um/h,525 C
FWHM (meV)
30.0
25.0
20.0
15.0
10.0
5.0
0.0
0.50
0.55
0.60
0.65
0.70
0.75
4K PL Peak Energy (eV)

Figure 8

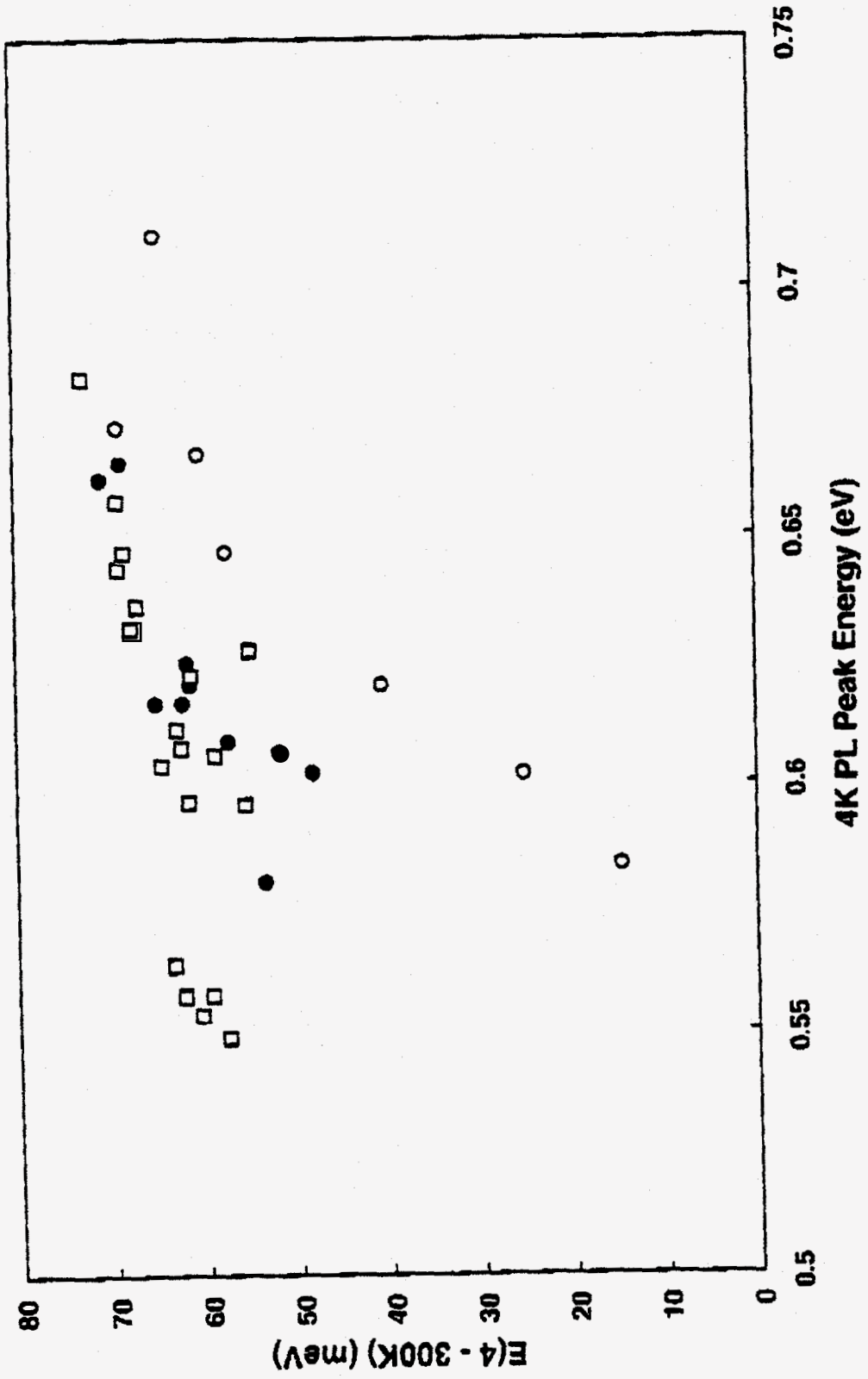
E(4 - 300K) (meV)
80
70
60
50
40
30
20
10
0
0.5
0.55
0.6
0.65
0.7
0.75
4K PL Peak Energy (eV)

Figure 9

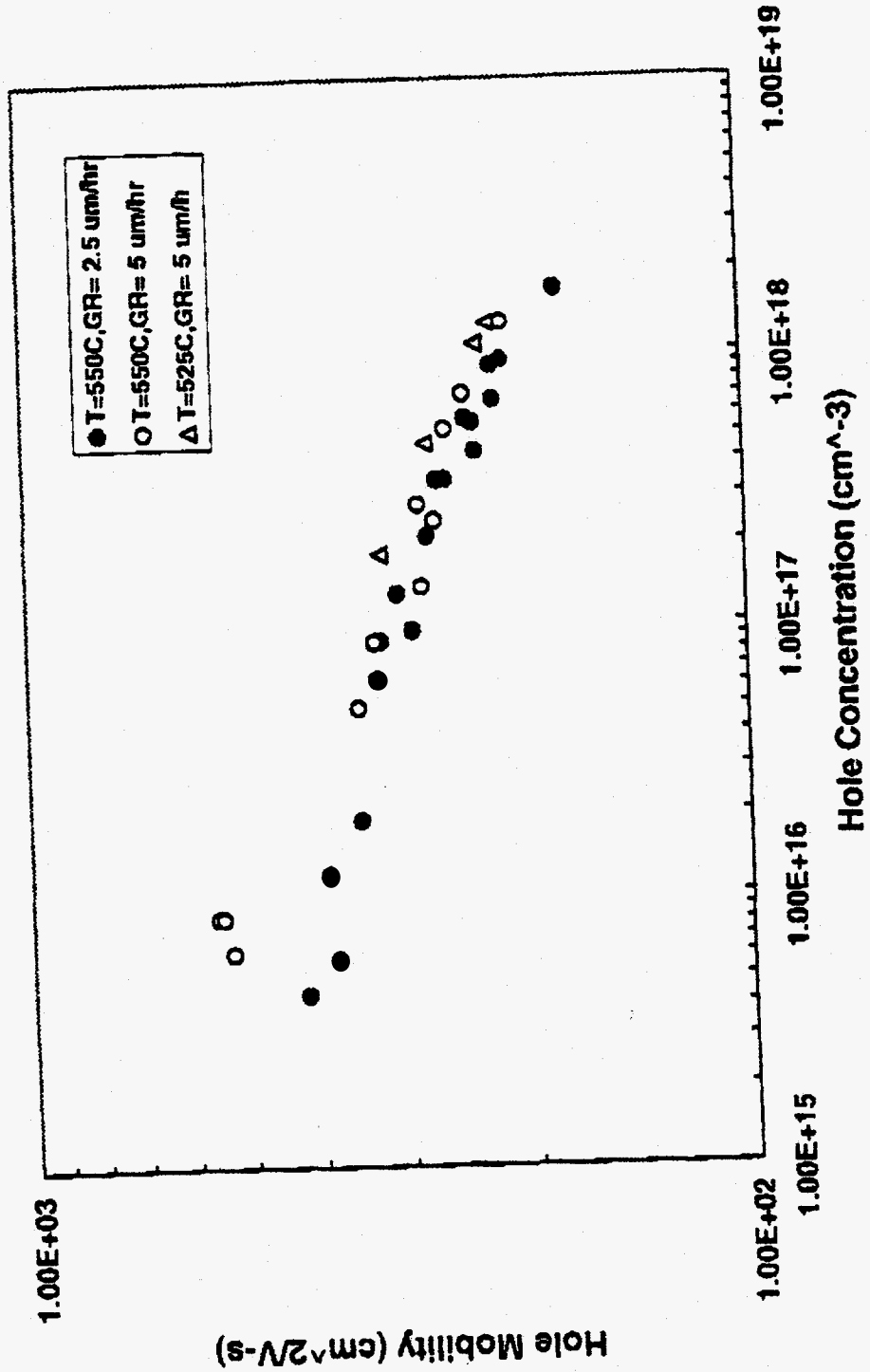
● T=550C,GR= 2.5 um/hr
○ T=550C,GR= 5 um/hr
Δ T=525C,GR= 5 um/h
Hole Mobility (cm^2/V-s)
1.00E+03
1.00E+02
1.00E+15
1.00E+16
1.00E+17
1.00E+18
1.00E+19
Hole Concentration (cm^-3)

Figure 10a

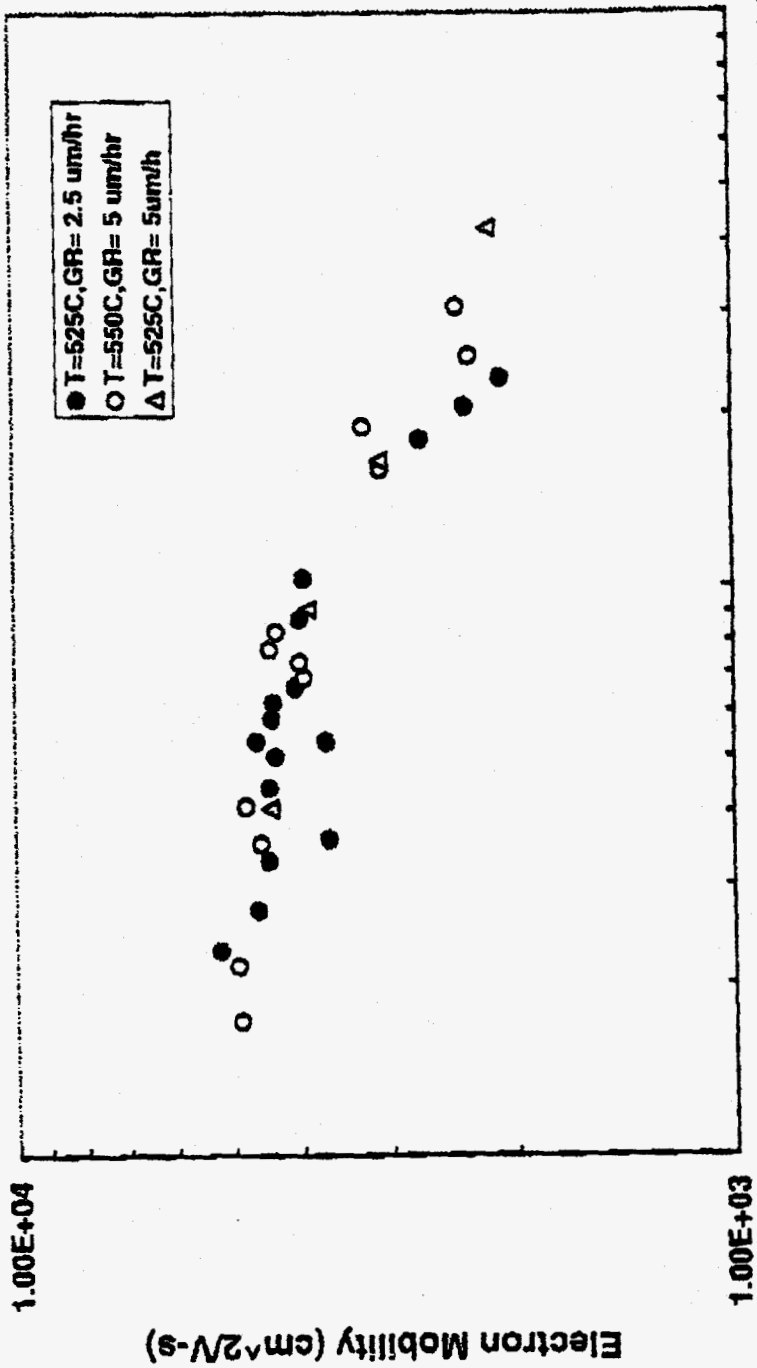
● T=525C,GR= 2.5 um/hr
○ T=550C,GR= 5 um/hr
Δ T=525C,GR= 5um/h
Electron Mobility (cm^2/V-s)
1.00E+04
1.00E+03
1.00E+17
1.00E+18
1.00E+19
Electron Concentration (cm^-3)

Figure 10b

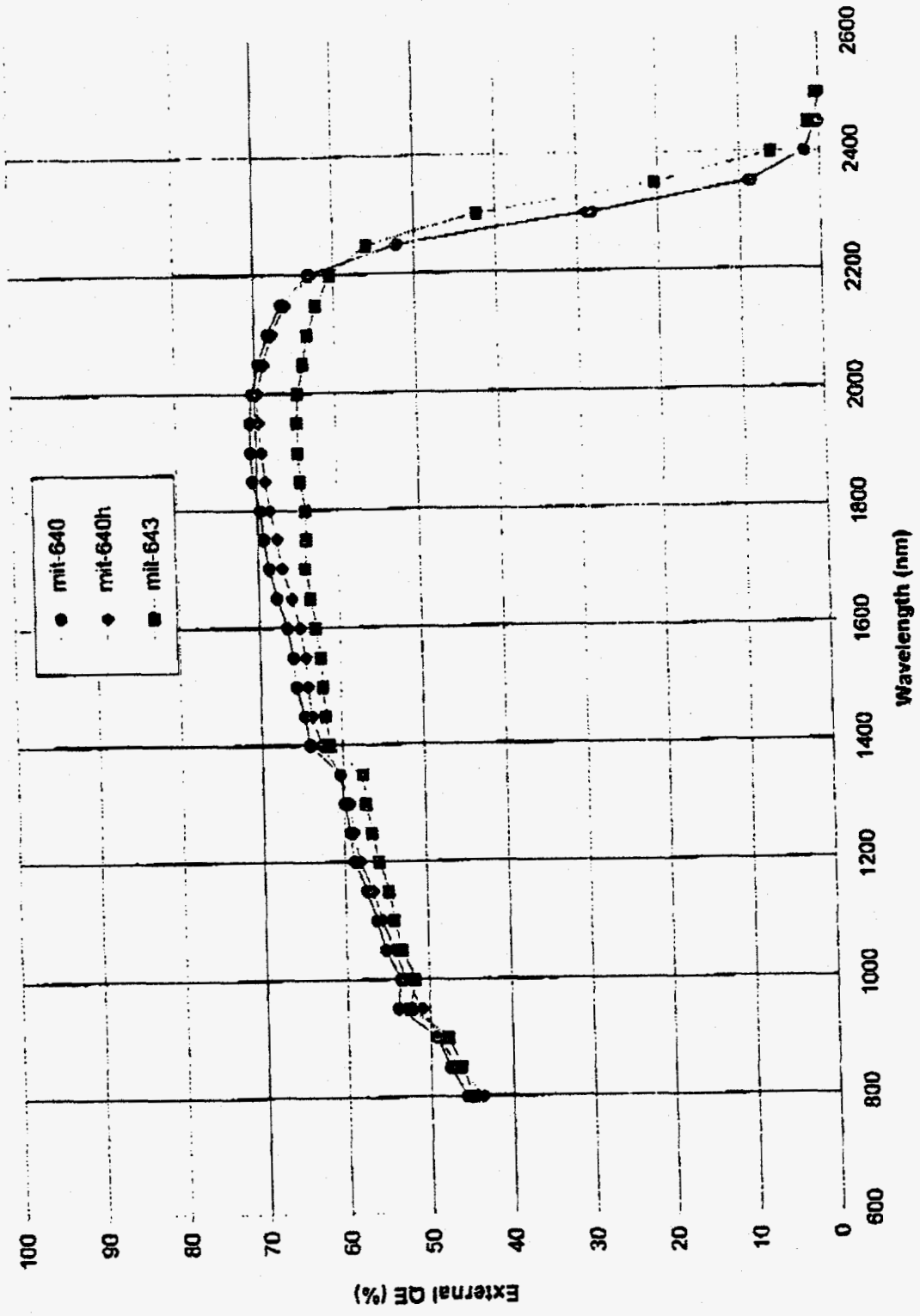
mit-640
mit-640h
mit-643
External QE (%)
Wavelength (nm)
100
90
80
70
60
50
40
30
20
10
0
600
800
1000
1200
1400
1600
1800
2000
2200
2400
2600

Figure 11

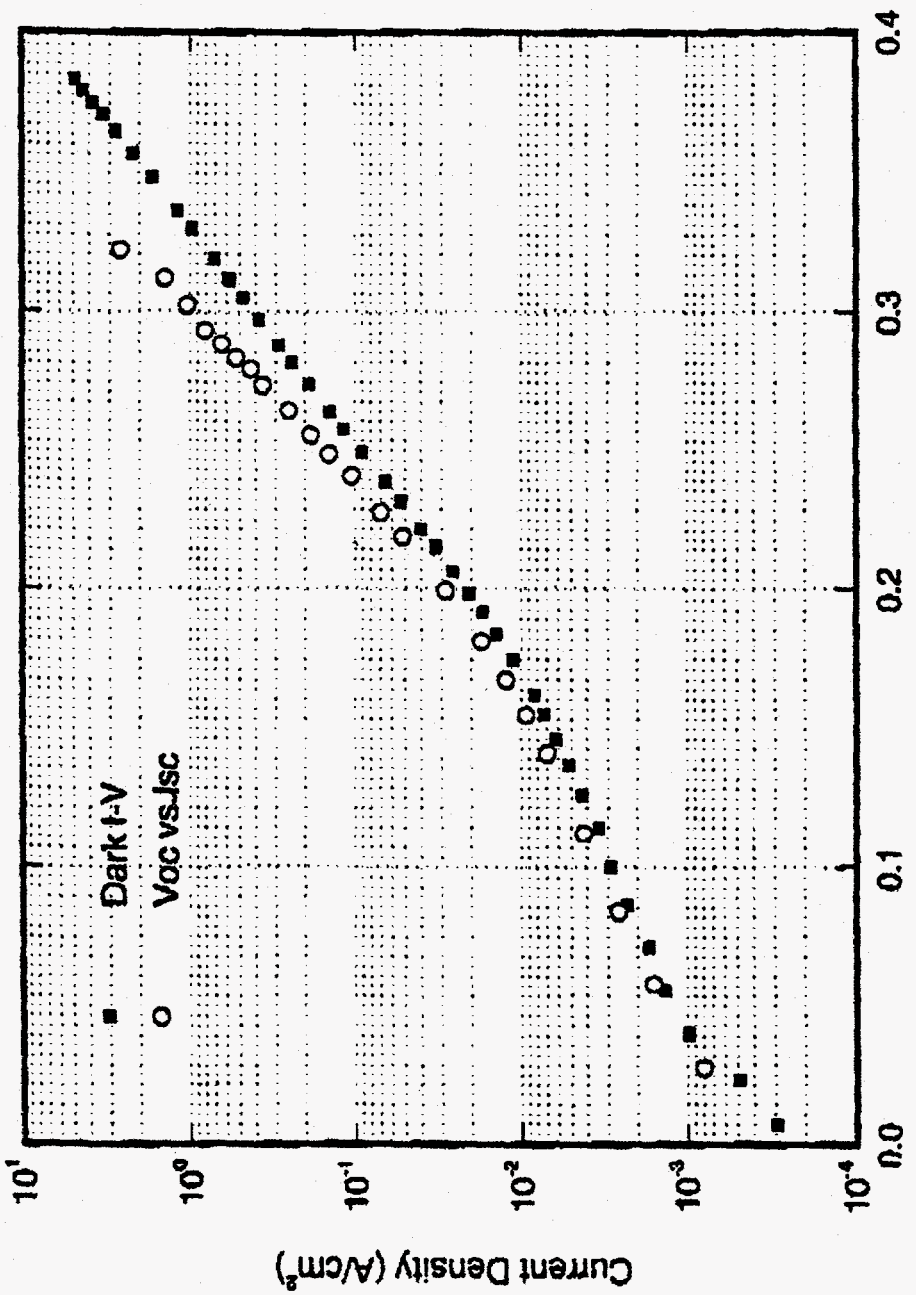
Dark I-V
Voc vs Jsc
Current Density (A/cm²)
Voltage (V)
10¹
10⁰
10⁻¹
10⁻²
10⁻³
10⁻⁴
0.0
0.1
0.2
0.3
0.4

Figure 12